MULTIPLE ELEMENT INTERFEROMETER FOR LOCATING SOURCES OF SOLAR NOISE AT 4,000 MEGACYCLES (I)

HARUO TANAKA AND TAKAKIYO KAKINUMA

Summary—With the intention of locating sources of solar noise at 4,000 MC, an interferometer with 5 aerials has been constructed. Each aerial has a paraboloidal reflector of size 1.5 meter in diameter, which can automatically follow the sun. Aerials are placed in E-W direction at 6 metre intervals. The main lobes are 43′ apart and have half-power widths of 7.8′. The output of each aerial is connected with waveguides and magic Tees and is led into the radiometer. General design principles and results of observations are described in this paper.

From the eclipse observations on Feb. 14, 1953, it is concluded that the radio disk of the sun is about 1.06 times larger than the optical one. In associated with the record of interferometer, we supposed a simple model about the radio distribution on the quiet solar disk, that is, the 6% excess region is 2.5 times brighter than the optical disk of the uniform temperature of 1.9×10^4 degree K.

The aerials of the interferometer are expected to be increased to 8-element in spring, 1954. At the same time, quarter-wavelength plates will be set up for the observation of polarized waves.

I. Introduction

It is one of the important problems in the field of radio astronomy to observe the distribution of noise sources over the solar disk at various frequencies. The study in this field has not yet been fully developed, however, as it is generally difficult to realize radio beams sharp enough to scan the sun directly.

The only means we can use is to apply the well-known interferometer method. An interferometer produces many lobes; but as the noise sources are restricted in a small region, each lobe can separately be used if no adjacent lobes do not fall on that area at a time. When a source extremely dominates the background radiation as is often the case at meter wavelengths, it can be located by two-aerial interferometer with different aerial spacings. On the other hand, as the abnormal sources do not dominate the background radiation at decimetre or centimetre wavelengths, multiple element interferometer must be used to determine the complete distribution of noise sources over the solar disk.

A 32 element interferometer for use at 21 cm has been constructed in Australia,[1] and has also been reported that an auxiliary N-S aerial group is now under construction. It has also been reported that a slotted waveguide with one directional horn for use at 10 cm has been constructed in Canada.[2]

Prior to these informations, we have started to construct 5-element interferometer for use at 7.5 cm and finished in March, 1953.[3][4] These aerials are expected to be increased to 8-element in spring, 1954.[5] The half-power beamwidth will then be 4.5 minutes of arc. At the same time, quarter-wave length plates will be set up to observe circularly polarized waves from individual sources.

Details of the equipment and the results of the primary observations are related in this paper. Some calculations are performed on the radio brightness distribution over the sun's disk, showing the existence of 'limb-brightening' which might be ascertained in more detail after the completion of 8-element aerials.

II. Design and Construction of Aerial Systems

1. Number of aerials and aerial spacings

Principles of the interferometer are the same as those of the optical diffraction gratings. Assuming that an interferometer consists of m nondirective aerials arranged in E-W direction at l metre intervals as shown in Fig. 1, its normalized power pattern can be represented as follows:

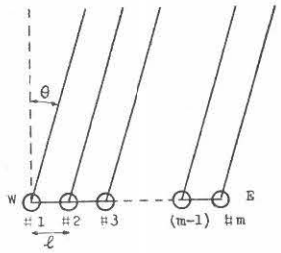

FIG. 1. Arrangement of aerials.

$$P=\frac{1}{m^2}\,\frac{\sin^2(\pi lm\sin\theta/\lambda)}{\sin^2(\pi l\sin\theta/\lambda)}. \tag{1}$$

Denote here that $\theta=\theta_p$ at the maximum response and $\theta=\theta_q$ at $P=0$,

$$\left.\begin{aligned}&\sin\theta_p=p\lambda/l && p=0,1,2,\ldots\\ &\sin\theta_q=(p+q/m)\lambda/l && q=1,2,\ldots(m-1).\end{aligned}\right\} \tag{2}$$

As the sun passes through this pattern, it is scanned stripwise by each lobe in turn. When the aerials are

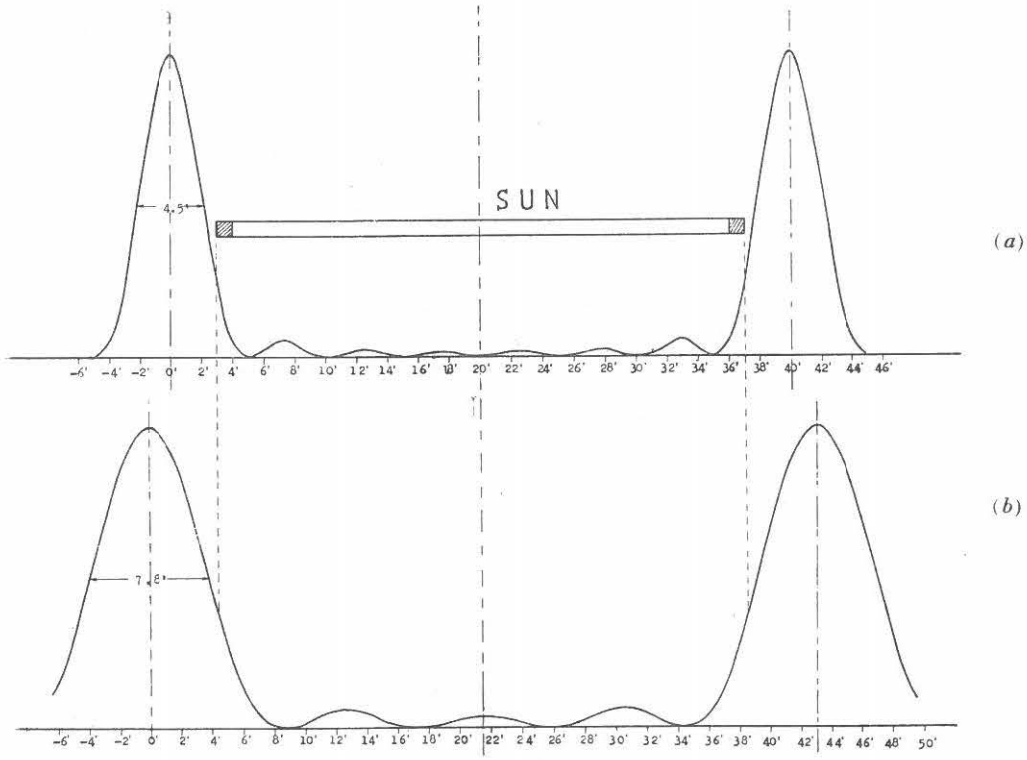

FIG. 2. Power pattern of 5-element (b) and 8-element (a) interferometer.

directive, equation (1) must be multiplied by their own pattern. As each aerial must have a large gain, consequently a high directivity at centimetre wavelengths, we can utilize only one or two fan-shaped beams with the fixed aerial system. Accordingly, aerials have to be constructed so as to be able to follow the sun.

The wider the aerial spacing, the smaller the angle between two beams and each beam becomes sharp as shown in Eq. (2). But as the aerial spacing must be so narrow that two beams do not scan the sun at a time, the number of aerials must be increased in order to obtain sufficient sharpness of the beams. If we use m aerials, we can divide the sun in m parts approximately.

As to the 5-element interferometer constructed, aerial spacings are 6 metre (80 wavelength), the lobes are spaced 43′ near the meridian passage and each lobe has a width of 7.76′ as shown in Fig. 2-(b). The 8-element interferometer to be constructed in near future will have the aerial spacings of 6.45 metre, (86 wavelength), lobe spacings of 40′ near meridian passage and half-power lobe widths of 4.5′, which are shown in Fig. 2-(a).

2. How to combine the input signal of each aerial and losses due to the combination

We have combined the input signals two by two with magic T. When a matched load is coupled to E-arm and two signals are fed to side arms respectively, the resultant signal comes out of H-arm. Unless the number of aerials is 2^n, we must insert losses properly in order to equalize the individual signals at the output of the last magic T. When the aerial system is composed of m elements, the coefficient of combination loss, L_c, is represented as follows;

$$L_c = m/2^{M+1},$$

where M is determined from the equation,

$$2^{M+1} \geqq m > 2^M.$$

For example, $L_c = 5/8$ for $m = 5$ and $L_c = 1$ for $m = 8$.

Moreover, as the signal is the noise of some bandwidth, each signal must be transmitted through the same course to the last magic T. Otherwise, we cannot obtain the pattern as shown in Fig. 1, and besides, we cannot keep the correct phase relations for the thermal expansion of transmission lines as well as for the minute variation of the frequency of local oscillator.

The arrangement for minimizing the length of total transmission lines in the case of 5-element interferometer is shown in Fig. 3-(a). Each signal is transmitted

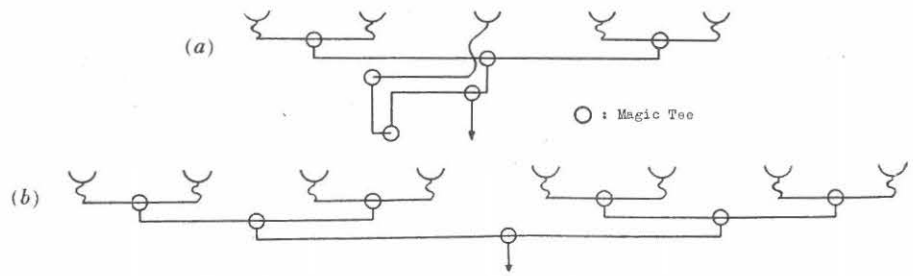

FIG. 3. The arrangement of transmission lines for 5-element (a) and 8-element (b) interferometer.

through 1 m coaxial cable, 3 magic T, 2 H-bends and 16 m waveguides to the input of the receiver. Two magic T, inserted in the equalizing path, are those to equalize losses by coupling matched loads to each one side arm.

In the case of 8 aerials, the arrangement is quite simple as shown in Fig. 3-(*b*).

3. Size of each aerial

In order to determine the size of an aerial, maximum signal in equivalent antenna temperature at the input of the receiver (T_5) must be compared with that of each aerial (T_1).

When 5 aerials are used, gain increases by 5 times; but receiving power decreases compared with an aerial with the same gain, because the interferometer has the sensitivity to only a part of the solar disk. A rate of decrease is about 0.3.

If the combination loss and the transmission losses (refer to III, 2) are taken into account, T_5 is about 0.7 T_1. As the r.m.s. fluctuation at the recorder is approximately 3° K for the bandwidth of 6 MC and the noise figure of about 15, it is desirable that T_5 is more than about 200° K. T_1 is then required to be about 300° K. Refering to our past data, we determined the size of the paraboloidal reflector of 1.5 m in diameter. Measurements show that T_1 is 288° K and T_5 is 189° K.

Owing to the combination loss (5/8), the transmission loss (1.34 db) and the leakage of earth's radiation (11° K), the background temperature at the input of the receiver is about 170° K when all aerials are directed toward zenith. As the result, recorder current alternates between two values corresponding to 160° K and 360° K approximately.

In the case of 8 aerials, these values will come to 100° K and 400° K respectively.

III. Details of the Equipment

1. Unit of the aerial system

A paraboroidal reflector as shown in Photo. 2, which has the aparture diameter of 151 cm, the angular aparture of 159° and the focal length of 45.3 cm, is made of aluminium with anticorrosive treatment.

Waveguide antenna feed, as shown in Fig. 4, has been chosen for its simplicity and to reduce the effect of rain-drops.

Gain of the aerial is 2,220 or 33.5 db, measured with the 2ry standard horn antenna. Directivity, measured with the sun as a signal source, is shown in Fig. 5.

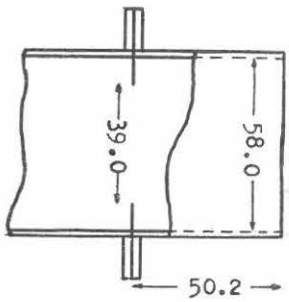

FIG. 4. Waveguide antenna feed

The polar axis of the equatorial mount can be steered automatically by a common shaft driven by a 15 w synchronous motor, which may be seen in Photo. 4. The common shaft can also be rotated reversely 20 times as fast as ordinary speed. Declination axis, on the other hand, must separately be adjusted by hand.

Parabolic mirror can be reinforced with stay, as shown in Fig. 6, when a storm threatens to come on.

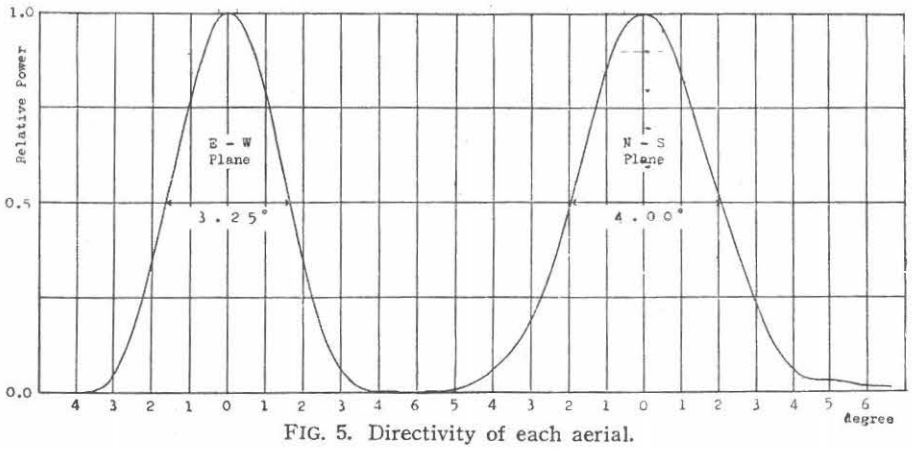

FIG. 5. Directivity of each aerial.

2. Transmission lines

The input of a feeding antenna is led through a curved waveguide as shown in Fig. 7 into a coaxial polyethyrene cable through a matched coupling (Fig. 8), placed near the cross point of polar and declination axes. After passing through one metre coaxial cable, the signal is again led into the waveguide feeder. The size of the waveguide feeder is shown in Fig. 9. Each signal passes here 3 magic *T* and 2 *H*-bends. All lines are kept off the direct sunlight and supported with rollers to prevent

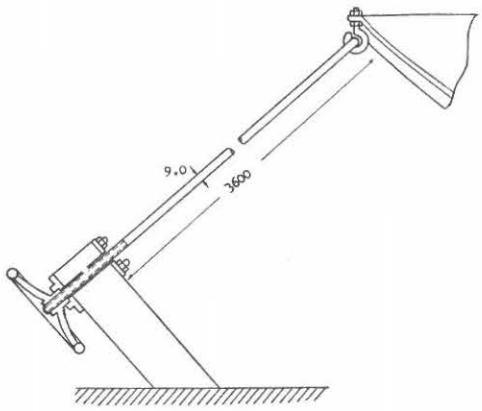

FIG. 6. Stay for a storm.

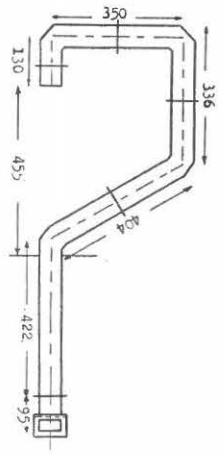

FIG. 7. The size of curved waveguide.

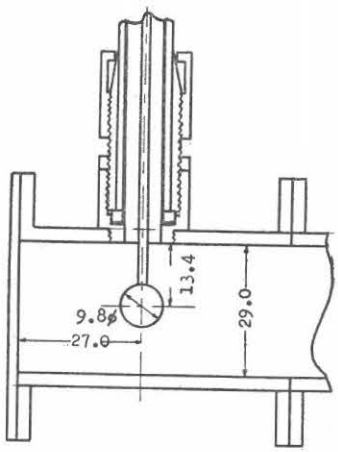

FIG. 8. Cable-waveguide connecter.

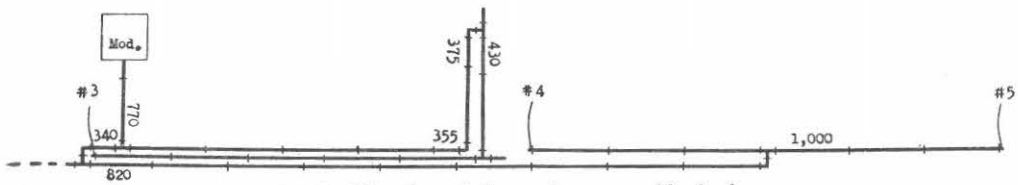

FIG. 9. The size of the main waveguide feeder.

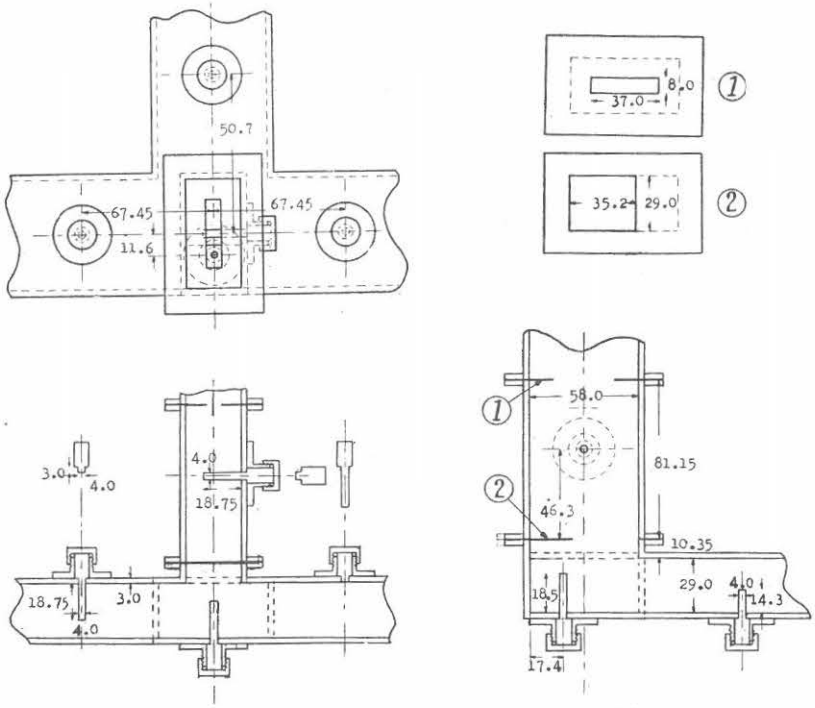

FIG. 10. Magic T for combining two signals.

stresses caused by temperature variations. Waveguides 58×29, which are made of copper and are coated with resin paint, have the transmission loss of about 0.036 db per meter, whereas coaxial cables have the loss of about 0.76 db per meter.

Fig. 10 shows the magic T used for combining two signals. It differs slightly from the conventional design, and the frequency characteristic of E arm is improved around the center as shown in Fig. 11. Moreover, it has switches to change it into a bend which allows to pass only one side of signals. This switch is used for the adjustment

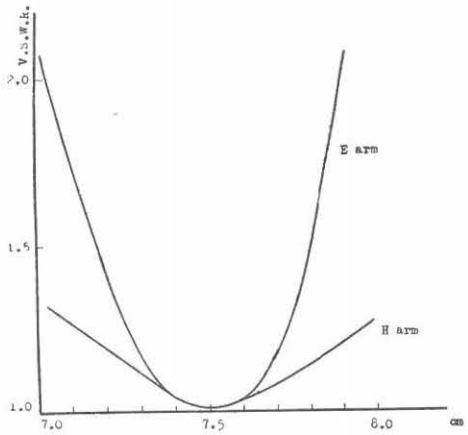

FIG. 11. Frequency characteristics of the magic T.

of aerial gain and phase relations to obtain sufficient deflections on the recorder.

3. Block diagram of the receiver

Fig. 12 shows the block diagram of the receiver, in which Dicke's modulation method is employed.

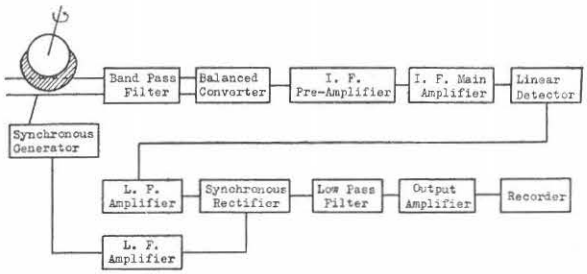

FIG. 12. Block diagram of the receiver.

4. S.H.F. part of the receiver

Modulator is almost the same as we have used in the radiometer for the intensity measurement at 3,750 MC.[6]

A filter for the rejection of image frequency is Fano-Lawson type[7] using stub reactances, which is shown in Fig. 13.

The frequency converter is a balanced type consisting of a magic T and two crystal mounts as shown in Fig. 14. The lengths of both side arms differ $\lambda_g/4$ each other and each converter unit is matched to the waveguide as good as below 1.1 in v.s.w.r. within the frequency range ± 60 MC.

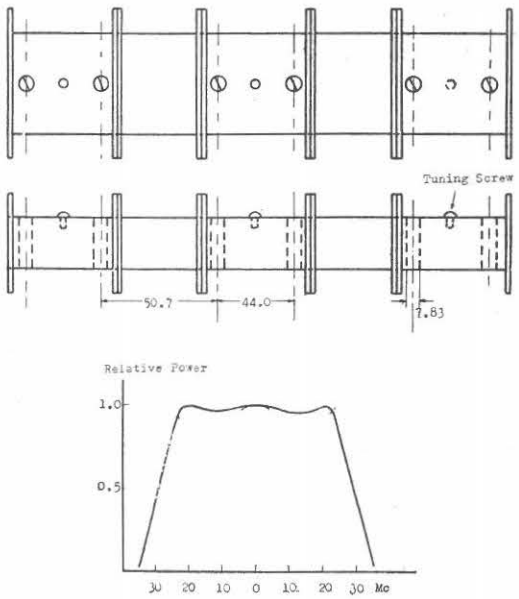

FIG. 13. Image rejection filter and its characteristic.

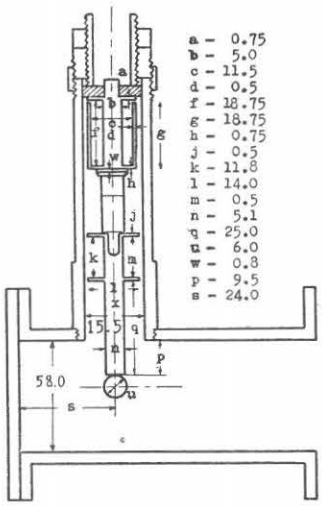

FIG. 14. Balanced frequency converter unit.

Stabilized local oscillator power is injected into E arm of the magic T. Stabilization is performed by means of a resonant high Q cavity as shown in Fig. 15, and the stability coefficient is about 10.

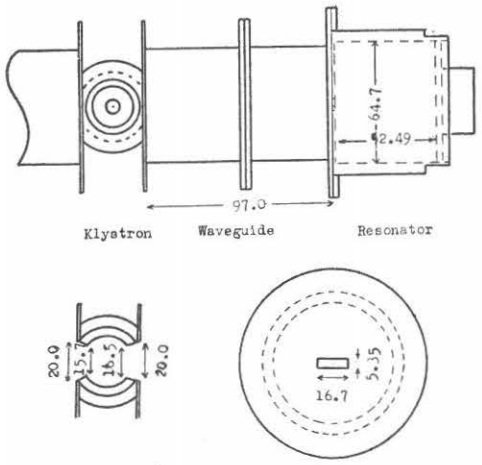

FIG. 15. Stabilization of a klystron oscillator.

5. I.F. and L.F. part of the receiver

As shown in Fig. 16, crystal mount is directly coupled to the *I.F.* input circuits, which are followed by a Wallman circuit. After a stage of triple stagger and a cathode follower, signal leaves the preamplifier and enters the level changer through 75 ohm coaxial cable. *I.F.* main amplifier consists of 2 triple staggers which is followed by a diode detector. The band-width measured with *S.H.F.* signal generator is 6 MC, and the overall noise figure is about 15.

L.F. circuits, shown in Fig. 17, are almost the same as has been described in the previous bulletin.[6] No frequency sensitive networks are used to keep sufficient stability against line frequency variations as well as temperature variations. Overall time constant is usually 1 second.

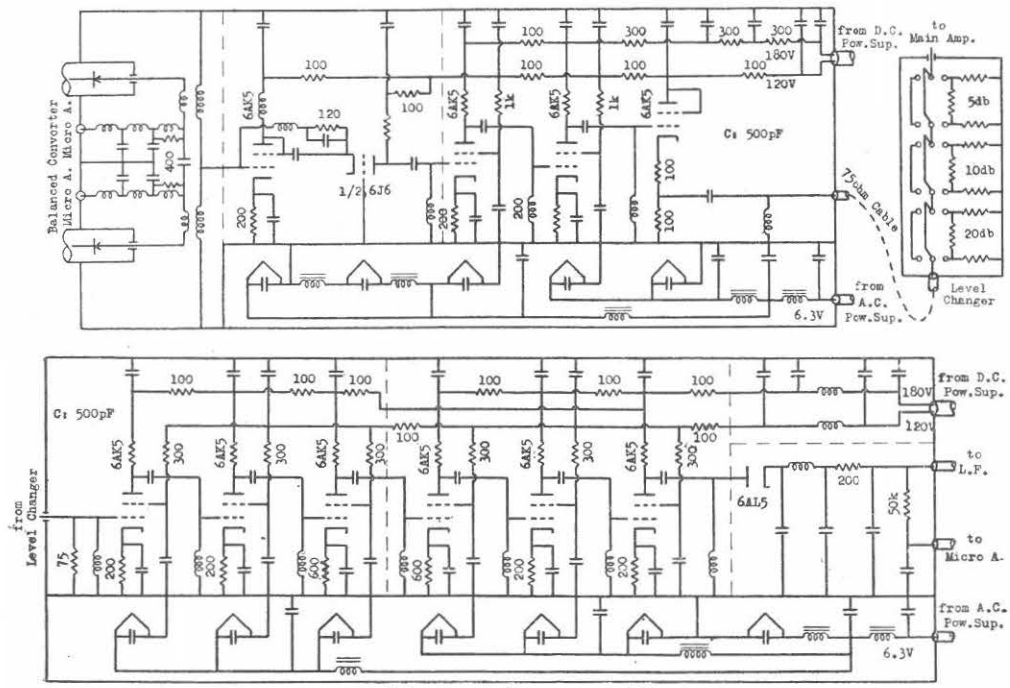

FIG. 16. Schematic diagram of *I.F.* circuits.

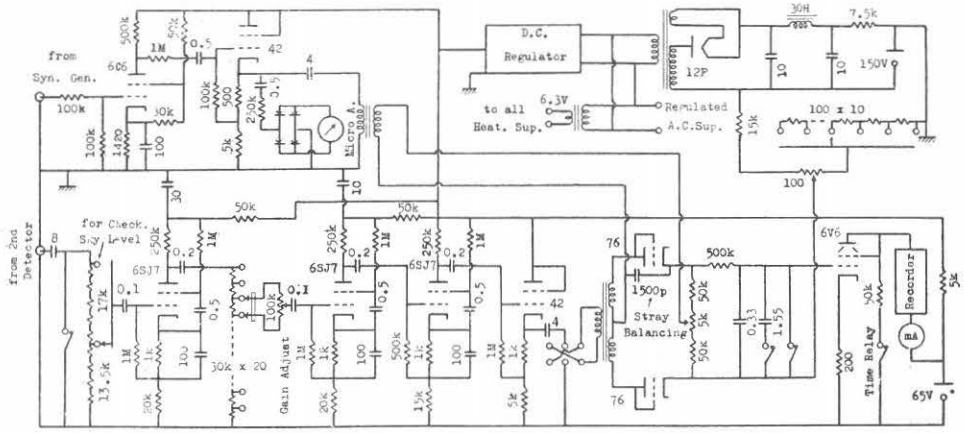

FIG. 17. Schematic diagram of *L.F.* circuits.

6. Standard 50 cycle power generator

To drive relay clocks and synchronous motors for steering parabolic mirrors, a standard frequency power generator is prepared (Fig. 18). A 120 KC crystal oscillator controls 4 stage demultiplier which is followed by an *R-C* oscillator for cleaning up the waveform. This standard frequency signal controls a thyratron inverter which can supply the power output of 100 watts.

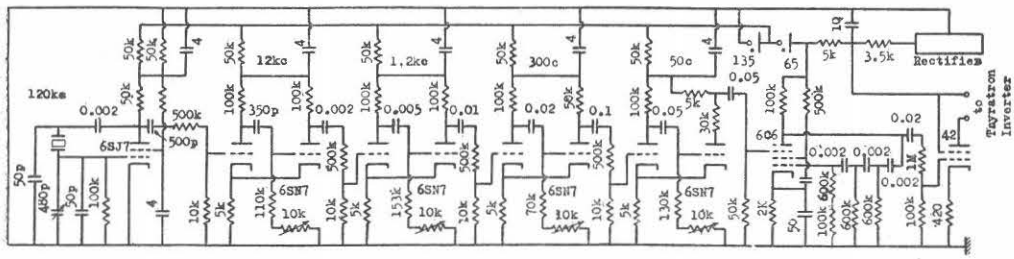

(*a*)

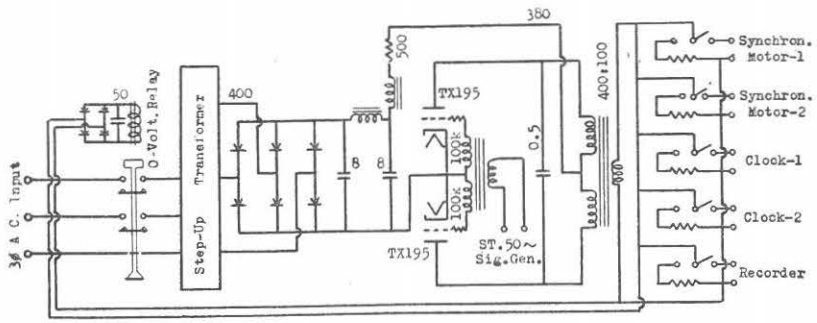

(*b*)

FIG. 18. Standard 50 cycle power generator.

7. Stabilized power supplies

A block diagram of power distribution circuits is shown in Fig. 19. Fig. 20 is the schematic diagram of power-line switches.

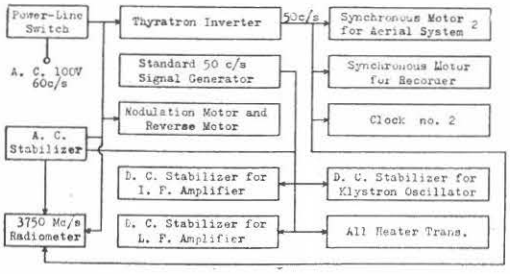

FIG. 19. Block diagram of distribution circuits.

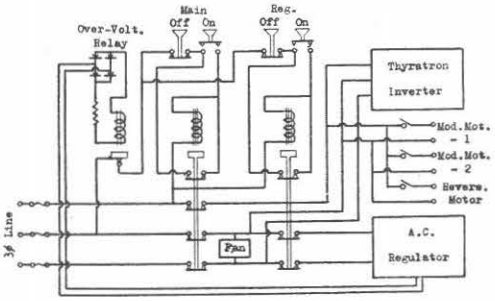

FIG. 20. Schematic diagram of power-line switches.

A.C. stabilizer, shown in Fig. 21, has the capacity of 1 KVA and keeps the effective value of the output voltage within 0.1 V for the line voltage variation between 85–110 V. Owing to a very thin tungsten filament and a high loop gain,

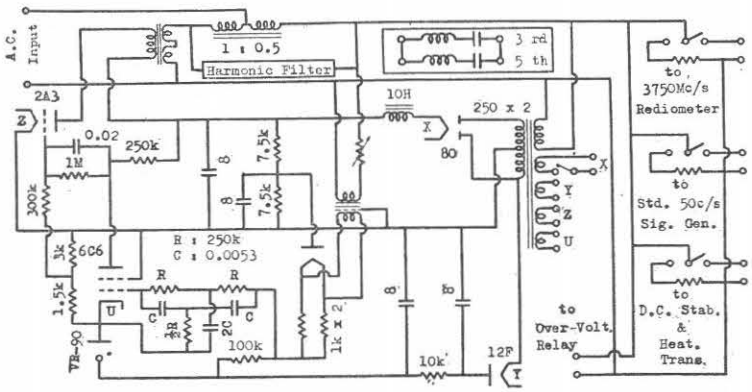

FIG. 21. *A.C.* stabilizer.

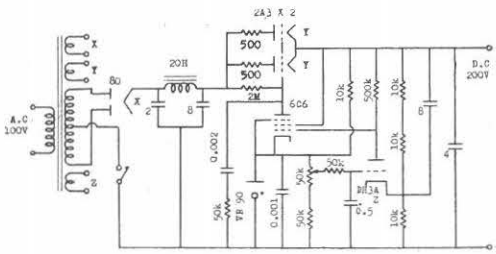

FIG. 22. *D.C.* stabilizer for *I.F.* amplifiers.

the transient response is as fast as below 0.1 second. Long time drifting caused by temperature variations of glow tube is about 0.3 volt.

D.C. stabilizer used for the *I.F.* amplifiers is shown in Fig. 22. *D.C.* stabilizer for *L.F.* circuits is the same as for the *I.F.* amplifiers except that 2A3 tube is single. As the loop gain is high, the output voltage is kept as constant as that of the standard glow tube.

A D.C. stabilizer for klystron oscillator is the same as described in Radiation Laboratory Series, Vol. 11, p. 53.

IV. Observational Techniques

1. Adjustment of phase relations

To adjust phase relations acculately, it is necessary to correct the lengths of waveguides experimentally. First of all, we direct 2 adjoining aerials toward the sun leaving others pointed at the zenith. If one of the maximum points of nearly sinusoidal interference pattern does not coincide with the time of meridian passage, we must correct the length of feeder on either side of aerials by calculations. For example, if the phase of the record leads 3.65°, we must add 1 mm waveguide on the west side of the feeder. Then we take a standard pattern over the whole time which concerns regular observations.

On the next day, we scan the sun each 2 or 3 times with adjoining 2 aerials successively and compare the records with those on the previous day. If the phases on the records are incorrect, the length of the feeder should be adjusted in same manner as before.

In these cases, switches of magic T are properly used to obtain sufficient deflections on the recorder.

2. Daily observations

We first preheat the equipment for more than an hour. Then we shortcircuit the input of the *L.F.* amplifier and set the deflection of the recorder at the point of room temperature (T_0° K) by adjusting bias of 6V6 tube. Returning the equipment to its ordinary state, we direct all the aerials toward zenith. Owing to the transmission losses, the combination loss and the leakage of aerial patterns to the earth, recorder should indicate the point $(0.54\,T_0+5)$° K, where we set the deflection by adjusting the amplifier gain. Aerials are then directed toward the sun.

Calibration of the equipment is performed at times with resistive loads, whose temperature is near 300° K and 600° K, in associated with large horn antenna, the noise temperature of which is near 0° K effectively. (Refer to p. 80.)

Time signals are inserted by a relay clock, which indicates noon at meridian passage.

3. Scanning velocity

As θ in Eq. (1) is not proportional to the angle of rotation around the polar axis (ψ) except near the vernal and autumnal equinox, the scanning velocity varies from day to day keeping the resolving power constant. Fig. 23 shows the relation between θ and ψ together with the position where each lobe falls on the centre of the sun.

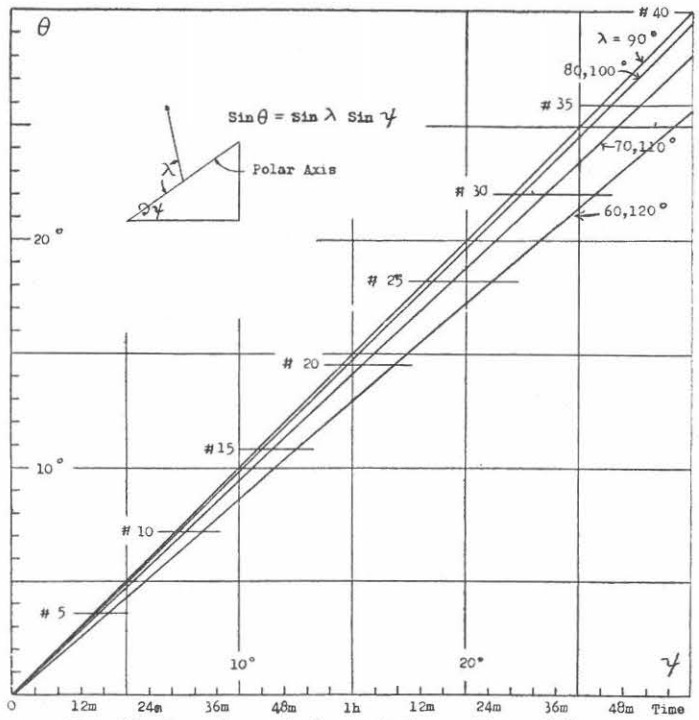

FIG. 23. Scanning velocity and the position of the sun.

4. Receiver bandwidth and hours of observations

When the receiver time constant is given, the output fluctuation of a radiometer is proportional to $F/\sqrt{B}$, where F is the overall noise figure and B is the bandwidth of the receiver. Accordingly, it is preferable to choose the receiver bandwidth as wide as possible in order to decrease the output fluctuations.

As to the interferometer performance, on the other hand, it may be considered that for wider bandwidths, the beam will become broad as θ increases, because the direction in which the maximum response occures varies with frequency in the same way as in the optical gratings. Nevertheless, we must conclude that this is not always true from the following reason.

Assume that the solar noise is Gaussian and the band shape of the receiver is rectangular with the bandwidth of B, the normalized power pattern of the aerial is represented as follows;

$$P=\frac{1}{m^2}\{m+2\sum_{\nu=1}^{m-1}(m-\nu)k_\nu\cos 2\pi\nu f_0\tau\} \tag{4}$$

where $\tau = l\sin\theta/c, \quad k_\nu = \sin\pi\nu B\tau/\nu\pi B\tau.$

If $k_\nu = 1$, Eq. (4) agrees with Eq. (1). Moreover, the change of beamwidth is negligible within the limit $k_\nu \fallingdotseq 1$ or $B\tau \ll 1$. In our case, in which $B = 6$ MC, the shape of even 60th beam ($\theta \fallingdotseq 48°$) is almost unchanged, though the amplitude decreases a little from the ideal case (Fig. 24).

The receiver bandwidth should rather be determined from the point of signal to noise ratio at the output.

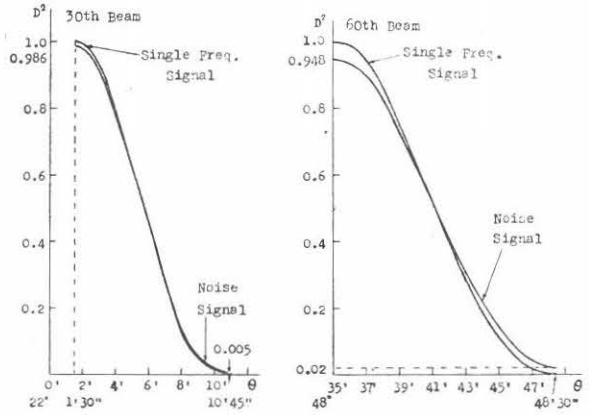

FIG. 24. Power pattern for the noise signal.

Though the beamwidth is almost unaffected by the receiving bandwidth, it becomes essentially dull as θ increases (see Eq. 2 and Fig. 2). Accordingly, the hours of observation are restricted to about one or two hours before and after the meridian passage. Were it allowed to confine the time of observation extremely short, we could receive two frequency bands on both sides of the local oscillator frequency to improve the effective noise figure of the receiver by about 3 db.

V. Records of Observations

An example of records obtained from primary observations is shown in Photo. 8. Fig. 25 shows the copy of these records picked up from daily data, refering to about five records around the local noon. The data in November are less accurate due to the irregular motion of recorder papers. Dotted lines indicate the minimum level corresponding to the quiet radiation. This minimum level of each month was traced after the method used by W. N. Christiansen,[1] that is, it is the lower envelope of the superimposed daily records during the month. These minimum levels are nearly consistent except the gradual change of time scale.

The positions on the solar disk of the bright areas are indicated by peaks on the records, which move as the sun rotates.

Radio records are refered to some results of the optical observations at the Tokyo Astronomical Observatory, as shown in Fig. 25. The grater part of the radio bright areas agrees with the sunspots. Some bright areas, on the other hand, can be seen at the position of the sunspots appeared on the other days. (e. g. June. 24., Sept. 7, Oct. 3, Oct. 25, Nov. 5. etc.)

VI. Distribution of Radio Brightness on the Quiet Solar Disk

1. Partial eclipse on Feb. 14, 1953.

Radio observations of partial eclipse at 3,750 MC was made here at Toyokawa, near Nagoya in Japan (137°22′5″ E, 34°50′6″ N). The intensity variation of the solar noise during the eclipse is shown in Fig. 26, all times being Universal time. (Refer to p. 89.)

It will be observed that: (1) the radio eclipse commenced about three minutes before the optical eclipse and ended after the same time, that is, the radio disk is larger than the optical disk; (2) the time of maximum obscuration does not agree

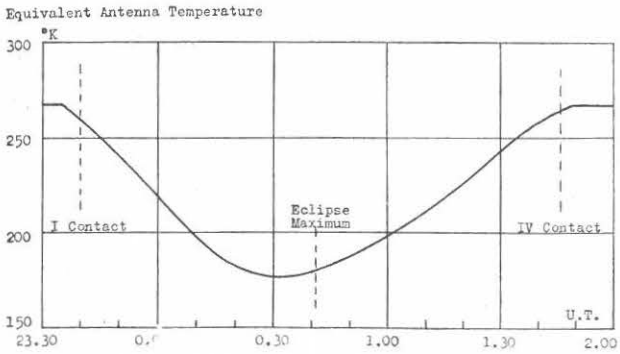

FIG. 26. Record of partial eclipse on Feb. 14, 1953.

with the time of minimum intensity, that is, there were some active zones on the sun which were obscured at the earlier time.

Daily observations of solar noise at this frequency have been made since Nov. 1951. Daily values during 6 months from Jan. to June, 1953 are shown in Fig. 27.

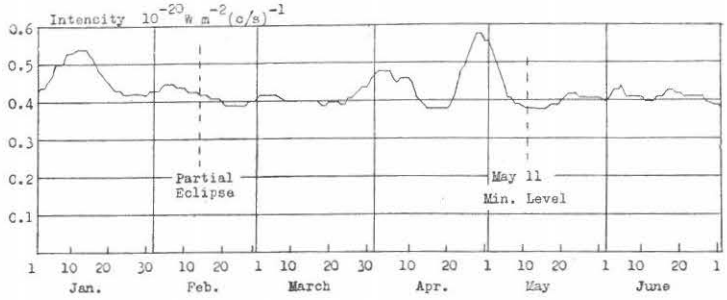

FIG. 27. Daily values of solar noise around the eclipse.

The intensity reached the minimum value $0.375 \times 10^{-20} WM^{-2}(c/s)^{-1}$ on May 11-15, 1953, which has not been exceeded till now. The daily value on the day of the eclipse was 0.42 in the same unit and it may be well supposed that there were some active zones on that day.

The distribution of sun-spots on the solar disk on Feb. 14 is supposed to be as shown in Fig. 28. It is based on the observation at the Tokyo Astronomical Observatory on Feb. 12, as it was cloudy on the day of eclipse.

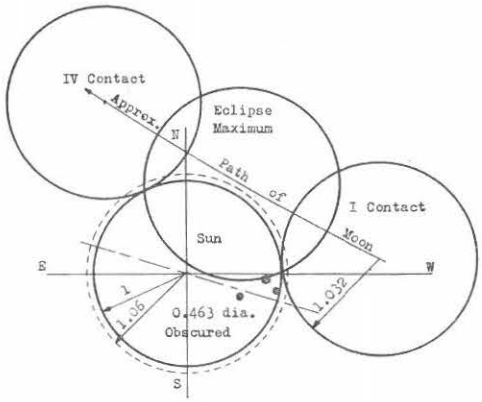

FIG. 28. Circumstances of eclipse and sun-spots.

The distribution of radio brightness on the quiet solar disk could be determined from the later half of these observations, but it is too delicate to do so under these circumstances of eclipse. It may be concluded, however, that the radio disk is 1.06 times larger than the optical one.

2. Calculations from the record of interferometer when the sun is quiet

In order to determine the distribution of radio brightness on the quiet solar disk, one had best wait until the sun becomes quiet. Fortunately, the records of the interferometer showed that the sun was almost quiet on May 11 and 12, that is, the records were almost unchanged and symmetrical. The intensity of radiation at 3,750 MC was also minimum on these days, as related previously. Hence, we used the average of some patters on these days for calculations about the quiet sun.

As mentioned in sec. V, the recorder pattern of each month corresponding to the quiet radiation was traced and was compared with the above pattern. We could find no difference among them within the accuracy of observations.

Assume that the distribution of the sun's equivalent temperature T is radially symmetrical, the receiving power N of 5-element interferometer can be represented approximately as follows;

$$N \propto \int_0^{\alpha}\int_0^{2\pi} \frac{\sin^2(5\pi l \sin\theta/\lambda)}{\sin^2(\pi l \sin\theta/\lambda)} T(r)\cdot r\cdot dr\cdot d\varphi \qquad (5)$$

where α is the visual radius of the radio frequency disk, and we consider only the case when the sun passes near the meridian. When the sun is in the direction of angle χ from the meridian, $\theta \fallingdotseq \chi + r\cos\varphi$.

Using Eq. (5), we calculated the theoretical record patterns for some simple models of various distributions and compared them with the experimental result. These curves are shown in Fig. 29. In this figure, (*a*) is the experimental curve, (*b*) corresponds to uniform distribution over the optical disk ($\alpha = 16'$) and (*c*) corresponds to uniform distribution over the disk whose radius is 1.06 times larger than the optical one. The experimental curve agrees with curve (*d*). which is drawn on the assumption that the radio disk is 1.06 times larger than the optical one and that the exess region is about 2.5 times brighter than the optical disk of uniform temperature. This assumption can also fully explain the variation of radio intensities during the later part of the eclipse (Fig. 30).

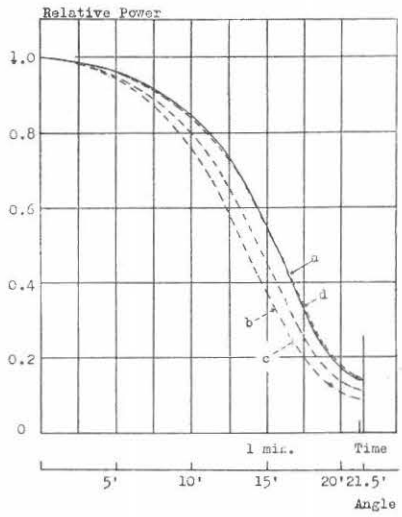

FIG. 29. Theoretical and experimental record patters.

In Fig. 30, the theoretical curve *b* does not coincide with curve *a*, in which the effect of active zones is contained. But as shown in Fig. 28, it may be considered that during the later half of the eclipse, no active zones were obscured. Accordingly, subtracting the amount increased by active zones from the observational values ($0.42 - 0.375 \times 10^{-20}\ \mathrm{W}m^{-2}\ (\mathrm{c/s})^{-1}$), we can obtain the curve *c* corresponding to the quiet sun. It agrees very closely with curve *b*.

We may conclude from this simple model that the radiation from the quiet sun consists of 23.6% from the limb and 76.4% from the uniform optical disk. The

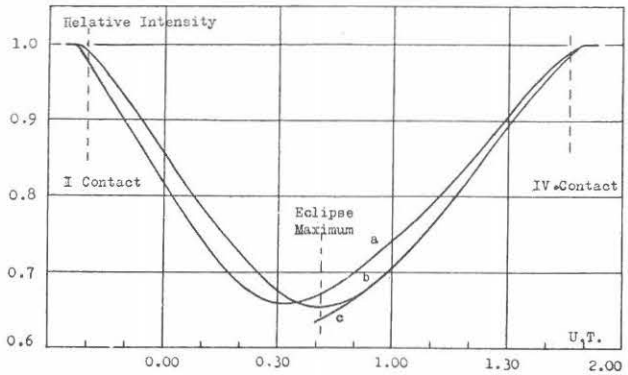

FIG. 30. Coincidence of theoretical and experimental curve on the later half of the eclipse.

equivalent temperature of this uniform disk is calculated to be about 1.9×10^4 degree K. at 4,000 MC.

VII. Acknowledgement

Authors are greatly indebted to Mr. S. Suzuki and his co-operators in the Tokyo Astronomical Observatory for their kindness in supplying astronomical informations.

We also wish to acknowledge to Mr. H. Jindo, T. Takayanagi and C. Torii for their enthusiastic assistance and careful observations for a long time.

We express, in conclusion, our cordial gratitude to Mr. A. Kimpara, director of the Research Institute of Atmospherics, Dr. Y. Hagiwara and other members of the National Commitee, U.R.S.I., in Japan for their incessant encouragement to our studies.

References

1) W. N. Christiansen and J. A. Warburton: The distribution of radio brightness over the solar disk at a wavelength of 21 centimetres. Aust. Jour. Phys., **6**, 2, June, (1953).
2) R. E. Williamson: Report of commission V of the national commitee, Canada Proc. General Assembly, U.R.S.I., **IX**, 6.
3) H. Tanaka and T. Kakinuma: Epuipment for locating sources of solar noise at 4,000 MC-(I). Bul. Res. Inst. Atmos., **3**, 1-2, Dec., (1952), in Japanese.
4) H. Tanaka and T. Kakinuma: Equipment for locating sources of solar noise at 4,000 MC-(II). Bul. Res. Inst. Atmos., **4**, 1, July, (1953), in Japanese.
5) H. Tanaka and T. Kakinuma: Equipment for locating. sources of solar noise at 4,000 MC-(III). But. Res. Inst. Atmos., **4**, 2, Jan., (1954), in Japanese.
6) H. Tanaka and T. Kakinuma: Equipment for the observation of solar noise at 3,750 MC/s. Proc. Res. Inst. Atmos., **1**, Jan., (1953).
7) R. M. Fano and A. W. Lawson: The theory of microwave filters. M.I.T. Rad. Lab. Ser., **9**, Chap. 9.

FIG. 25 (*a*). Superimpose daily records.

FIG. 25 (*b*). Daily records and optical sun-spots.

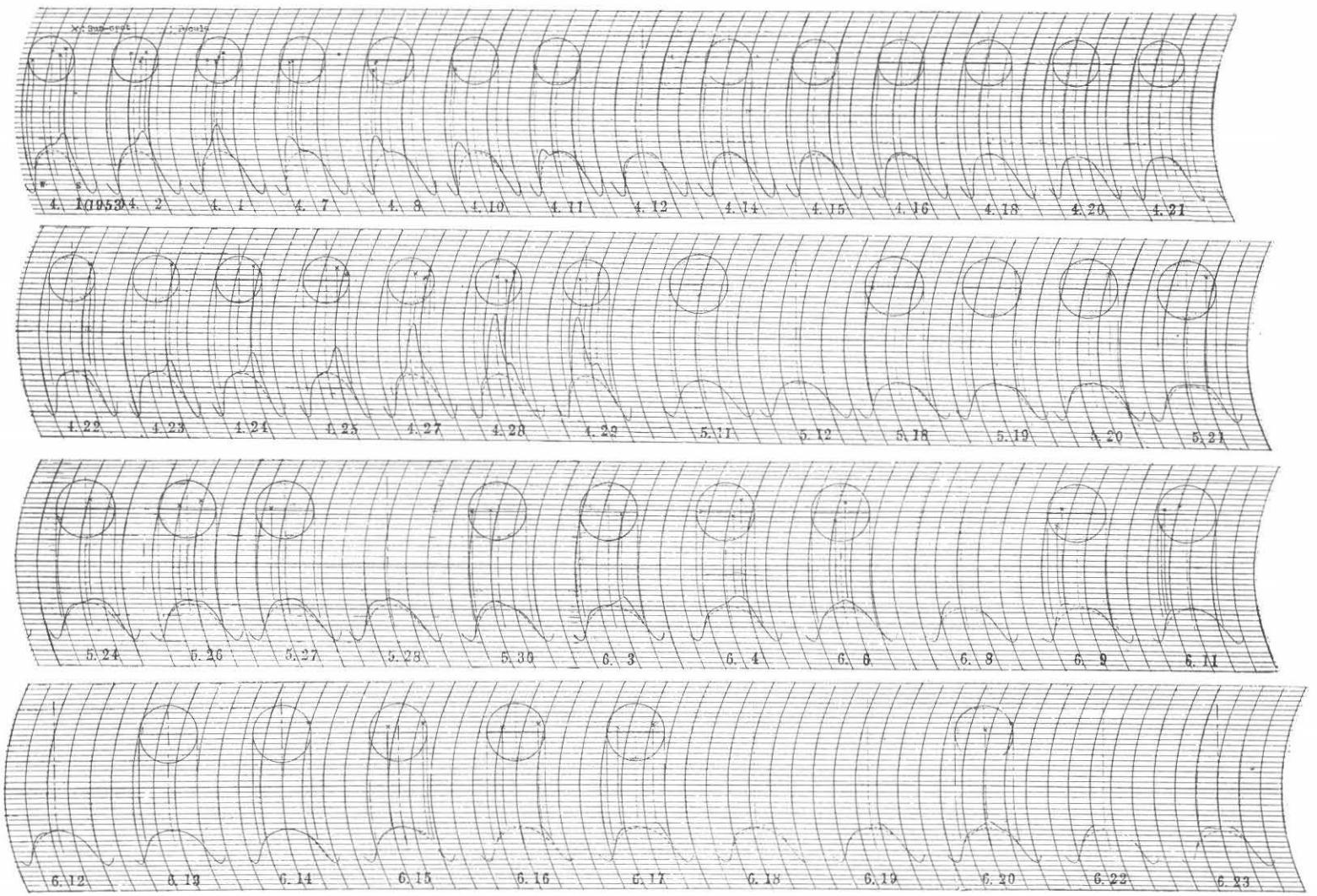

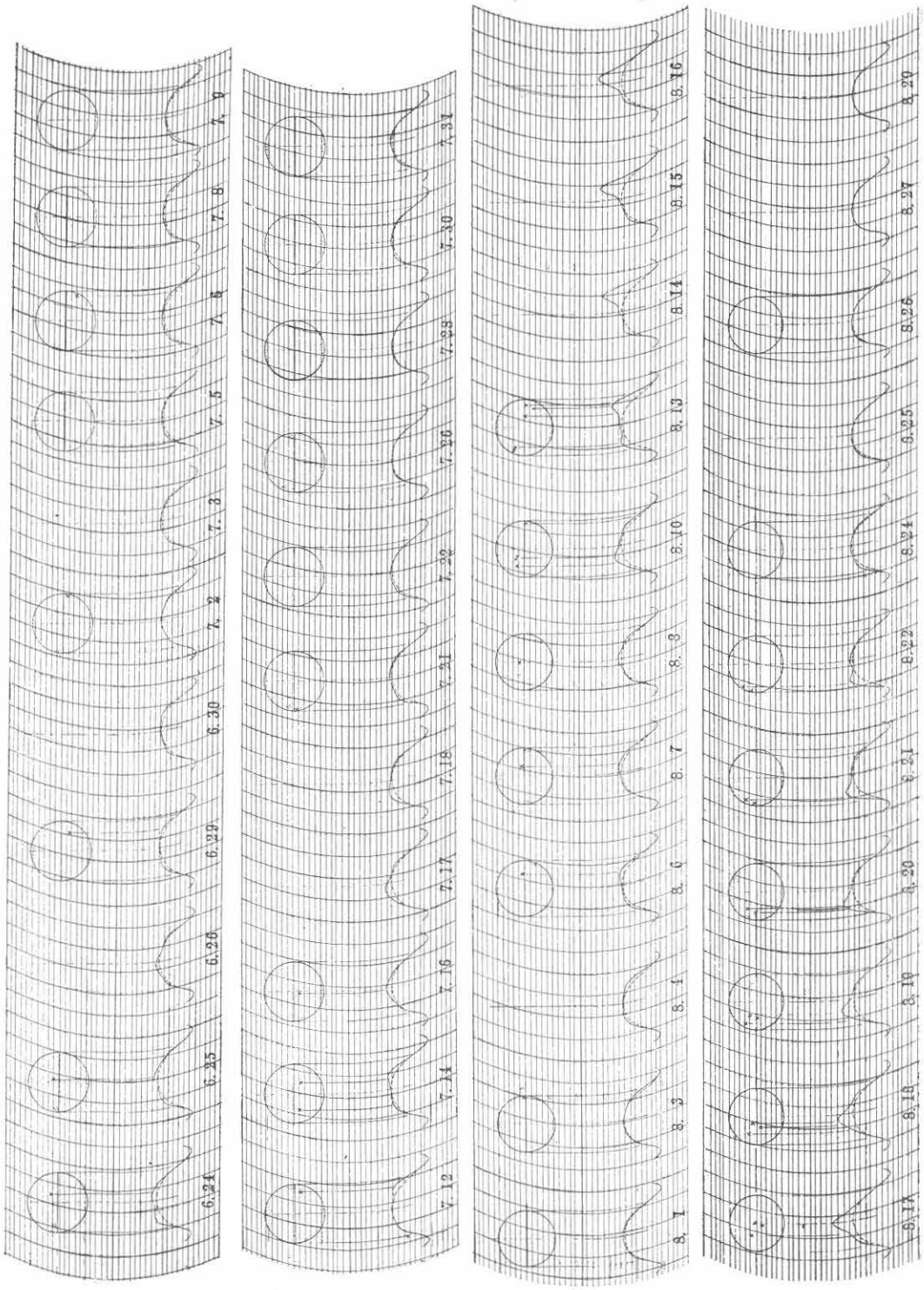
6.24
6.25
6.26
6.29
6.30
7. 2
7. 3
7. 5
7. 6
7. 8
7. 9
7.12
7.14
7.16
7.17
7.18
7.21
7.22
7.26
7.28
7.30
7.31
8. 1
8. 3
8. 6
8. 7
8. 8
8.10
8.13
8.14
8.15
8.16
8.17
8.18
8.19
8.20
8.21
8.22
8.24
8.25
8.26
8.27
8.29

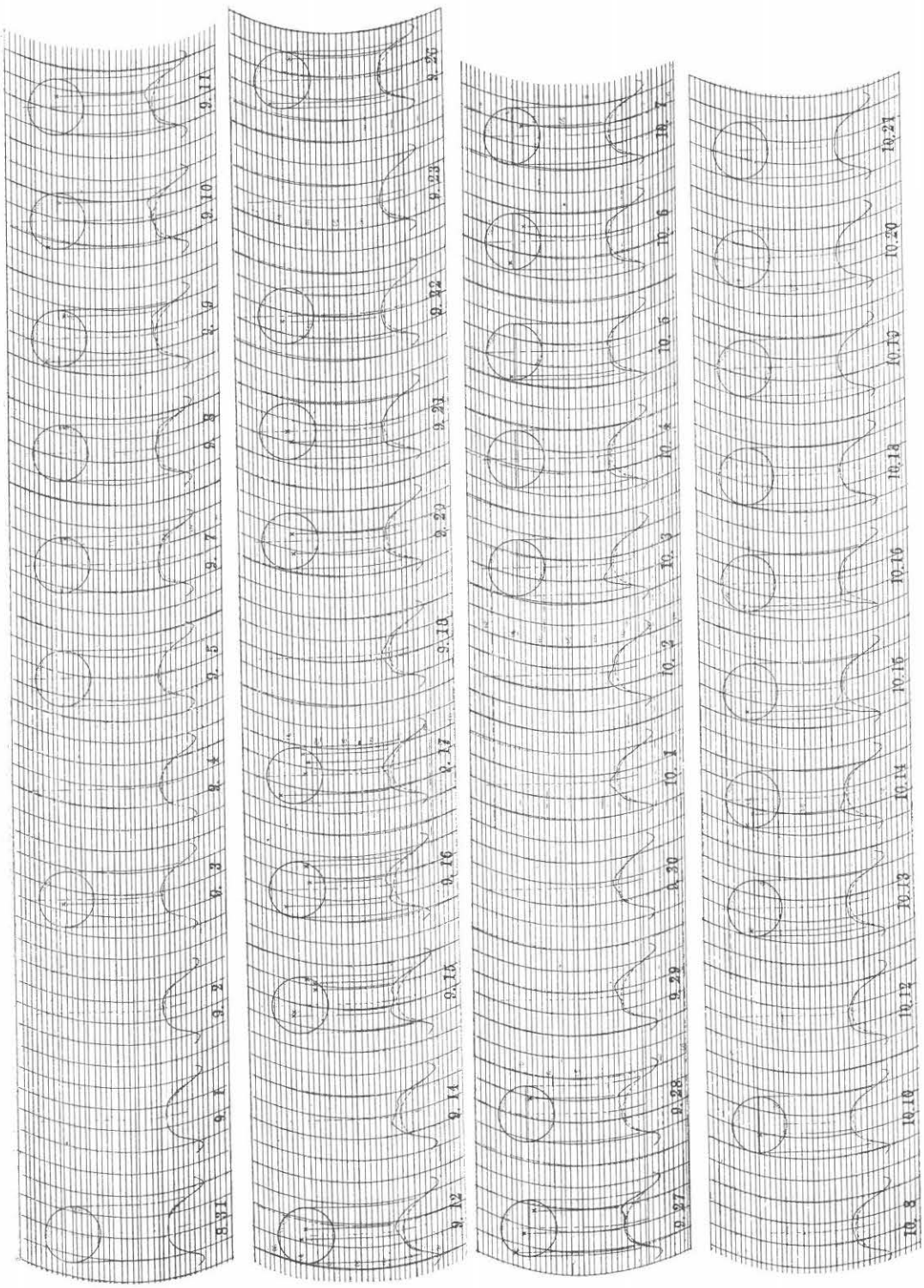
9.11
9.10
9. 9
9. 8
9. 7
9. 6
9. 5
9. 4
9. 3
9. 2
9. 1
8.81
9.12
9.14
9.15
9.16
9.17
9.18
9.19
9.20
9.21
9.22
9.23
9.24
9.25
10. 7
10. 6
10. 5
10. 4
10. 3
10. 2
10. 1
9.30
9.29
9.28
9.27
10.27
10.20
10.19
10.18
10.16
10.15
10.14
10.13
10.12
10.10
10. 8

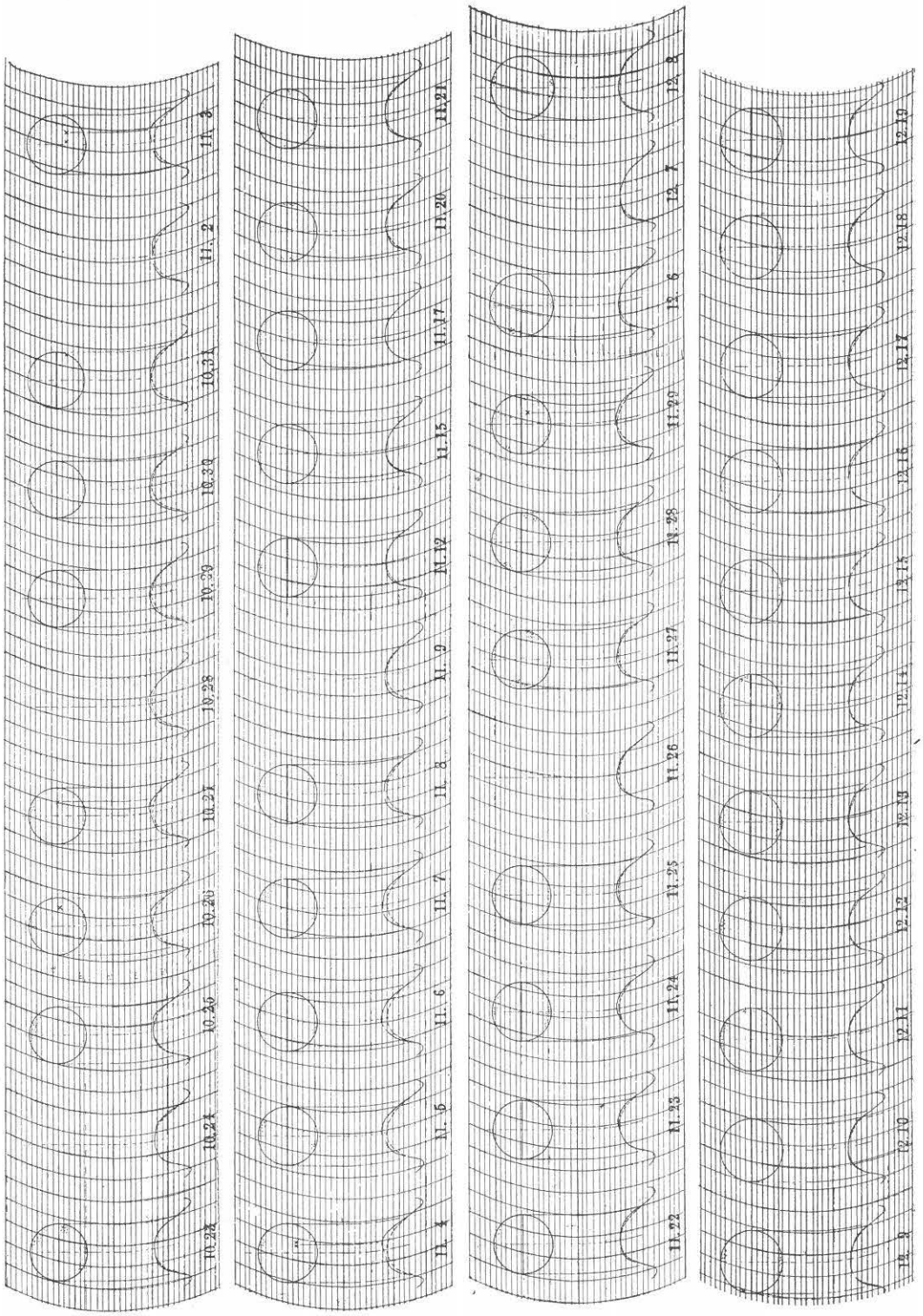
10.22
10.24
10.26
10.28
10.30
10.32
10. 2
10. 4
10. 6
10. 8
10.10
10.12
10.14
10.16
10.18
10.20
11. 1
11. 3
11. 5
11. 7
11. 9
11.11
11.13
11.15
11.17
11.19
11.21
11.23
11.25
11.27
11.29
11.31
12. 1
12. 3
12. 5
12. 7
12. 9
12.11
12.13
12.15
12.17
12.19
12.21
12.23
12.25
12.27
12.29
12.31
13. 2
13. 4
13. 6
13. 8
13.10
13.12
13.14
13.16
13.18
13.20
13.22
13.24
13.26
13.28
13.30
13.32
14. 1
14. 3
14. 5
14. 7
14. 9
14.11
14.13
14.15
14.17
14.19
14.21
14.23
14.25
14.27
14.29
14.31
15. 2
15. 4
15. 6
15. 8
15.10
15.12
15.14
15.16
15.18
15.20
15.22
15.24
15.26
15.28
15.30
15.32
16. 1
16. 3
16. 5
16. 7
16. 9
16.11
16.13
16.15
16.17
16.19
16.21
16.23
16.25
16.27
16.29
16.31
17. 2
17. 4
17. 6
17. 8
17.10
17.12
17.14
17.16
17.18
17.20
17.22
17.24
17.26
17.28
17.30
17.32
18. 1
18. 3
18. 5
18. 7
18. 9
18.11
18.13
18.15
18.17
18.19
18.21
18.23
18.25
18.27
18.29
18.31
19. 2
19. 4
19. 6
19. 8
19.10
19.12
19.14
19.16
19.18
19.20
19.22
19.24
19.26
19.28
19.30
19.32
20. 1
20. 3
20. 5
20. 7
20. 9
20.11
20.13
20.15
20.17
20.19
20.21
20.23
20.25
20.27
20.29
20.31
21. 2
21. 4
21. 6
21. 8
21.10
21.12
21.14
21.16
21.18
21.20
21.22
21.24
21.26
21.28
21.30
21.32
22. 1
22. 3
22. 5
22. 7
22. 9
22.11
22.13
22.15
22.17
22.19
22.21
22.23
22.25
22.27
22.29
22.31
23. 2
23. 4
23. 6
23. 8
23.10
23.12
23.14
23.16
23.18
23.20
23.22
23.24
23.26
23.28
23.30
23.32
24. 1
24. 3
24. 5
24. 7
24. 9
24.11
24.13
24.15
24.17
24.19
24.21
24.23
24.25
24.27
24.29
24.31
25. 2
25. 4
25. 6
25. 8
25.10
25.12
25.14
25.16
25.18
25.20
25.22
25.24
25.26
25.28
25.30
25.32
26. 1
26. 3
26. 5
26. 7
26. 9
26.11
26.13
26.15
26.17
26.19
26.21
26.23
26.25
26.27
26.29
26.31
27. 2
27. 4
27. 6
27. 8
27.10
27.12
27.14
27.16
27.18
27.20
27.22
27.24
27.26
27.28
27.30
27.32
28. 1
28. 3
28. 5
28. 7
28. 9
28.11
28.13
28.15
28.17
28.19
28.21
28.23
28.25
28.27
28.29
28.31
29. 2
29. 4
29. 6
29. 8
29.10
29.12
29.14
29.16
29.18
29.20
29.22
29.24
29.26
29.28
29.30
29.32
30. 1
30. 3
30. 5
30. 7
30. 9
30.11
30.13
30.15
30.17
30.19
30.21
30.23
30.25
30.27
30.29
30.31
31. 2
31. 4
31. 6
31. 8
31.10
31.12
31.14
31.16
31.18
31.20
31.22
31.24
31.26
31.28
31.30
31.32
32. 1
32. 3
32. 5
32. 7
32. 9
32.11
32.13
32.15
32.17
32.19
32.21
32.23
32.25
32.27
32.29
32.31

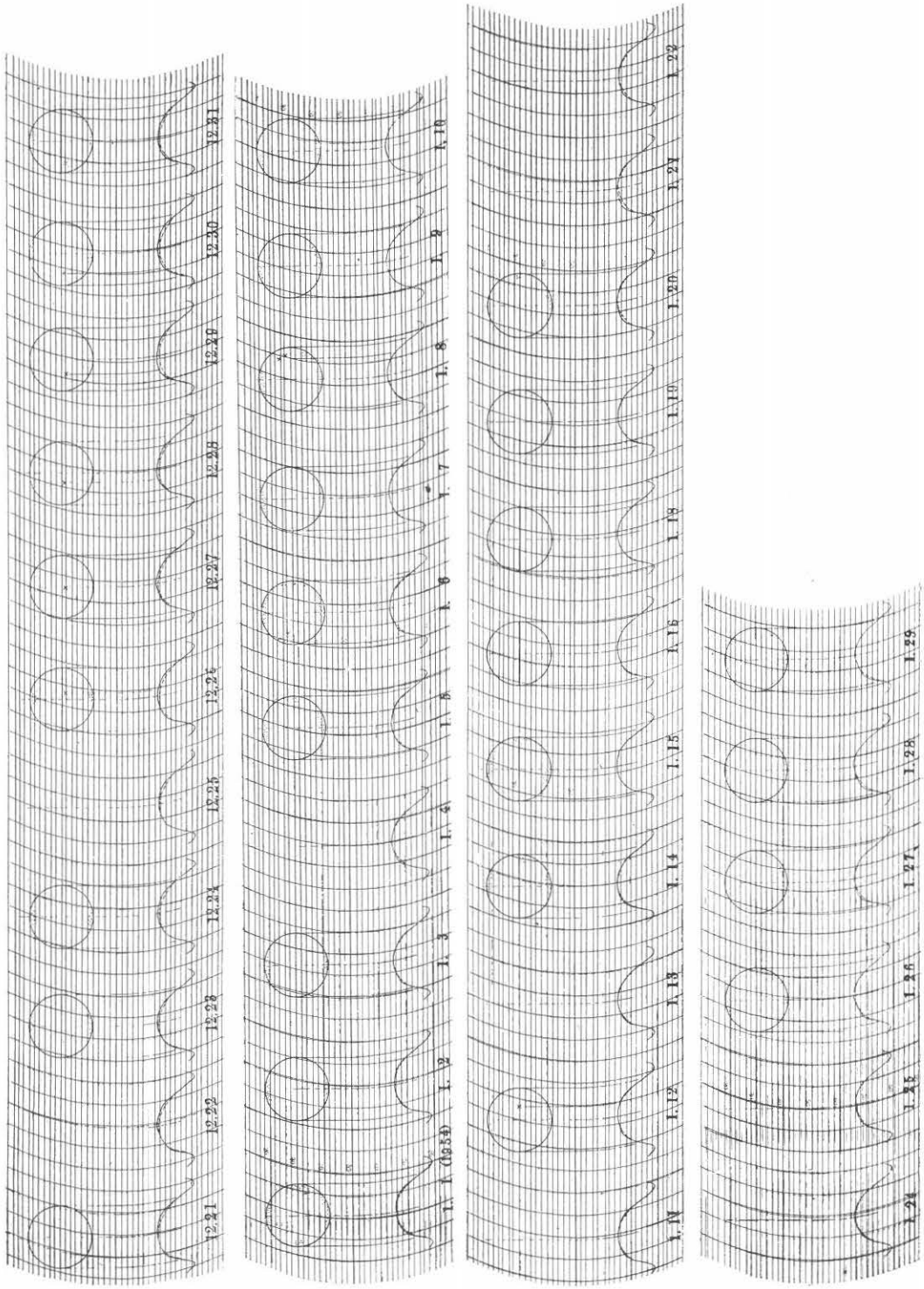
I.21
I.22
I.23
I.24
I.25
I.26
I.27
I.28
I.29
I.30
I.31
I.1 (1934)
I.2
I.3
I.4
I.5
I.6
I.7
I.8
I.9
I.10
I.11
I.12
I.13
I.14
I.15
I.16
I.17
I.18
I.19
I.20
I.21
I.22

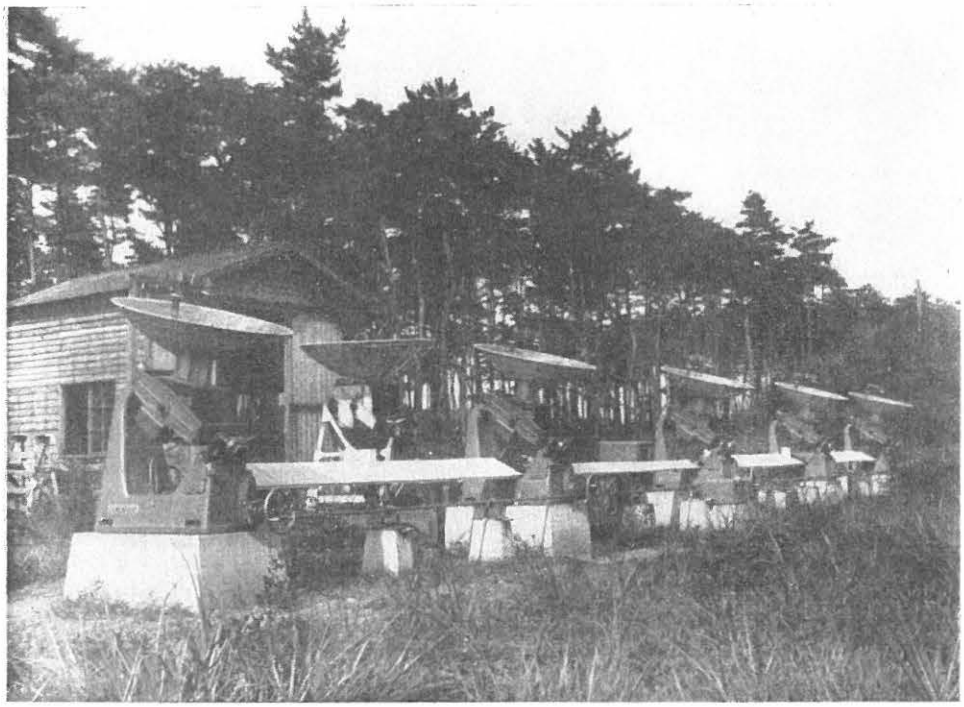

(*a*)

(*b*)

PHOTO. 1. The complete view of the aerial system.

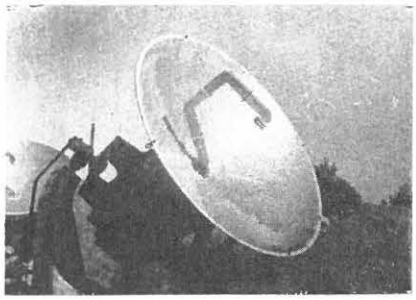

PHOTO. 2. Paraboloidal reflector and waveguide feed.

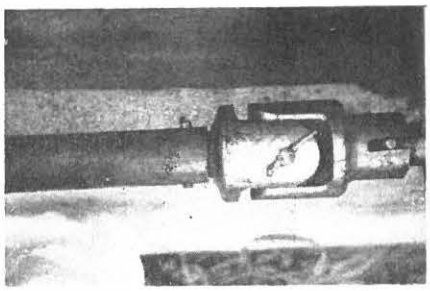

PHOTO. 5. Universal coupling of common shaft.

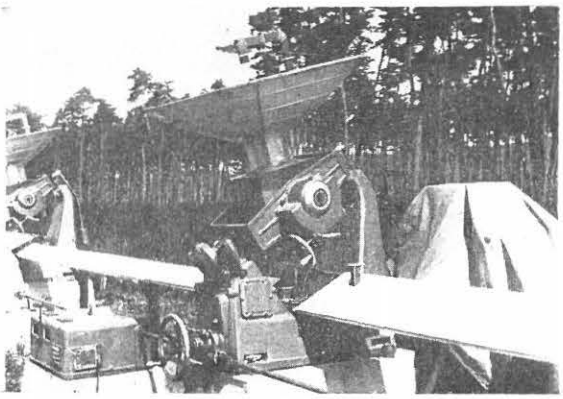

PHOTO. 3. Mount of the reflector.

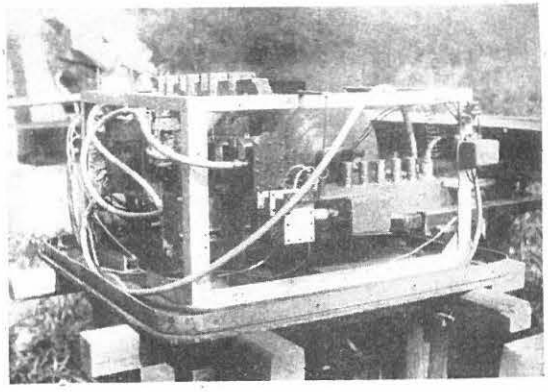

PHOTO. 6. The head of the reciver uncovered.

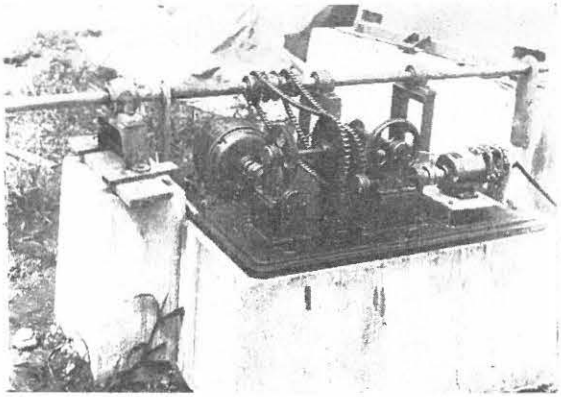

PHOTO. 4. Reduction gear uncovered.

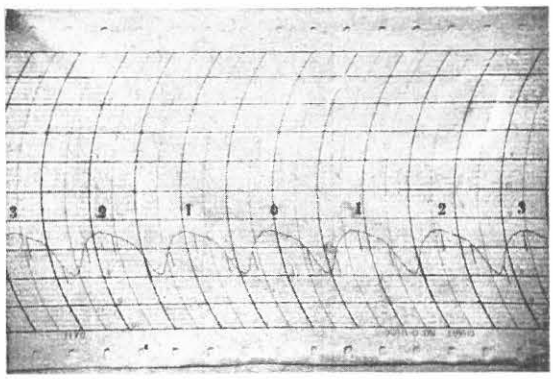

PHOTO. 8. The main part of the receiver.

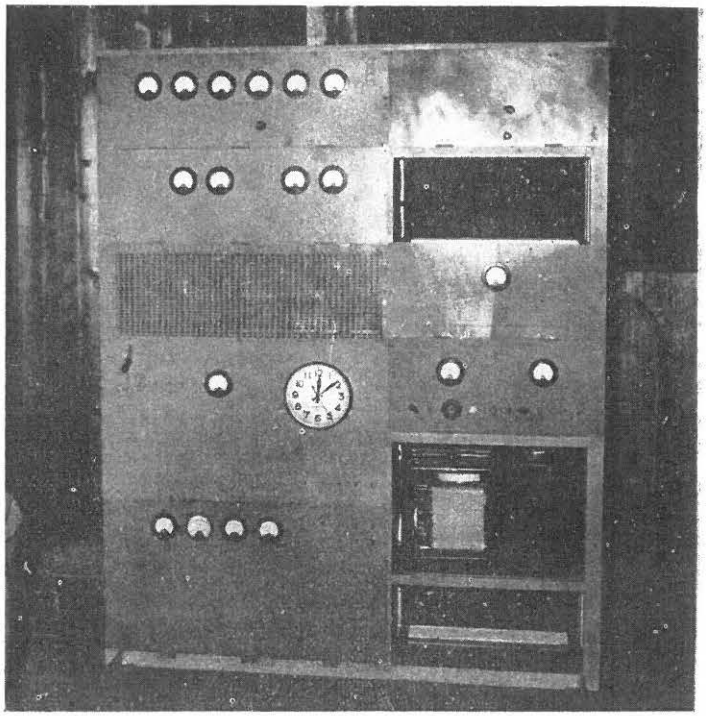

(*a*)

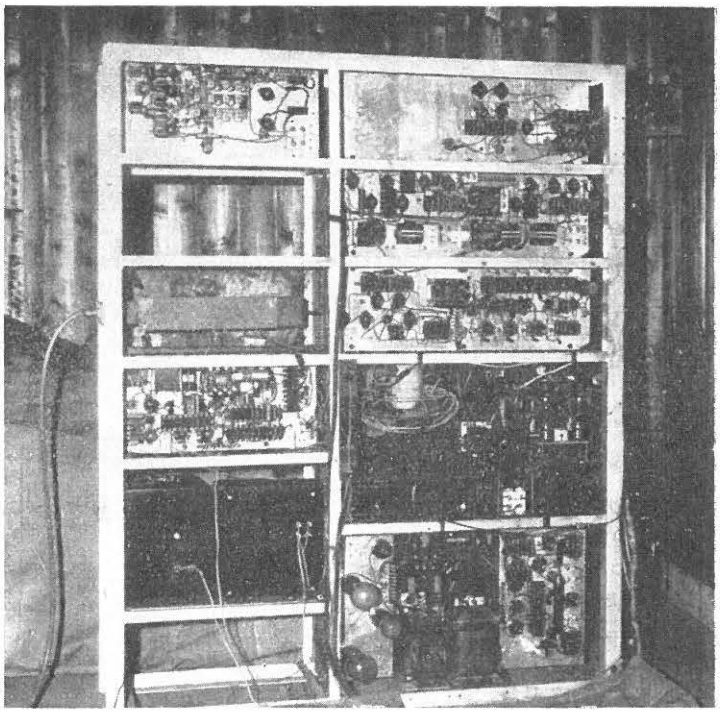

(*b*)

PHOTO. 7. An example of the record (May 31, 1953).